ISSN: 0975 -8542

Journal of Global Pharma Technology

Available Online at: www.jgpt.co.in

RESEARCH ARTICLE

Effect of Doped Nickel on the Structural and Electrical Properties of Alumina Prepared by the Chemical Co-precipitation Method

Omer H. Abas, Mehdi H. Diwan, Nabeel A. Bakr

Physics Department, College of Science, Diyala University, Diyala, Iraq.

Abstract

Pure α-Al_2O_3 compound and its nickel (Ni) composites were prepared with different weight ratios according to the formula $((NiO)_x (Al_2O_3)_{1-x})$, where (x = 0, 0.125, 0.25, 0.375, 0.50 g) through the chemical co-precipitation method. These were calcined at 1300 ℃, and the prepared samples were characterized using different techniques such as XRD and FT-IR spectroscopy. The investigation by X-ray diffraction (XRD) showed that the prepared α-Al_2O_3had only one pure phase of α-Al_2O_3 with a crystallite size of 33nm, while the $NiAl_2O_4$ composites were formed in different phases according to the weight ratios of the NiO used (NiO/$NiAl_2O_4$, $NiAl_2O_4$, Al_2O_3 / $NiAl_2O_4$). In addition, the crystallite sizes of the phases of the resulting composites ranged from 35 – 50nm, and increased with increasing NiO content. The best result was obtained for the $NiAl_2O_4$ composite at x = 0.25g, where the characterization by FT-IR spectroscopy showed that the pre-calcined composites at 500 ℃ initially formed the spinal phase of the doped composites, but the composites prepared at the final sintering temperature of 1300 ℃ formed the pure and spinal phases. The effective NiO_4group was formed at the tetragonal sites and a part of it was formed in the octahedral sites, while the effective group (AlO_6) was formed at the octahedral sites, thereby indicating that the material was in the spinal inverse and spinal phases. The A.C. conductivity indicated that the highest value of the dielectric constant was at a minimum frequency and decreased with increasing frequency at low frequencies as a result of the effect of a vacuum charge and ionic polarizations. However, at high frequencies, it was found that the dielectric constant did not depend on the frequency, thereby indicating that the dipole moments followed the electric field only at low frequencies. In addition, the A.C. conductivity showed that the conductivity increased with increases in the frequency according to the correlated barrier hopping model (CBH), where the charge carriers jump up from one site to another causing the A.C. conductivity to increase with increasing frequency

Key terms: *Nickel Alumina, Alumina, Dielectric, Precipitation method.*

Introduction

It is difficult to limit ceramic materials to a specific definition as they are multi-inorganic materials such as oxides, nitrides, and carbides that have a stable structural system and are able to withstand high temperatures [1, 2]. These materials have wide applications in many industrial fields because of their ability to withstand high temperatures and their high stability with regard to chemical materials [3, 4]. The outstanding characteristics of ceramic materials, namely, their hardness, low thermal and electrical conductivity, and tolerance of high temperatures, have made them of great importance in many industries and applications. Aluminium oxide is one of the most important ceramic materials with many applications because of its various characteristics such as optical transparency, high electrical and thermal insulation, and the fact that it is a stable chemical compound [5]. The importance of a doped alumina compound is characterized by a wide range of auxiliary factors. It can be processed at a low cost and with specific characteristics, including an increased surface area, as well as a precise balance in the formation of its surface (ACID-BASE), and the significant reinforcement of its mechanical properties [6,7]. $NiAl_2O_4$ is one of the most important alumina ceramic compounds, and it is used in many applications such as catalysts, pigments as well as magnetic materials [7-12]. This compound is attracting attention due to the possible formation of methane vapour as well as dry methane [12, 13, 15], which play a significant role in direct reduction in the production of active nickel

metal particles from $NiAl_2O_4$. It is necessary for the production and formation of layers in the spinal crystalline phase of the nickel-alumina composite from the traditional alumina compound with the help and support of the nickel element. In addition, a nickel-substituted alumina in the form of a nickel-alumina composite through re-oxidation is meant to improve the physical properties of the composite and produce active agents.

The presence of nickel-alumina layers prevents the calcinations and aggregation of nickel particles [17] which, in turn, will result in high stability with no carbon in the group. This is one of the main drawbacks in the simultaneous formation of a crystalline nickel-alumina composite system on the surface, which is considered to play an important role in increasing the high efficiency of the $NiAl_2O_4$ composite with the formation of methane vapour [17].Today, the $NiAl_2O_4$ composite is a potential alternative to the conventional alumina, with additional benefits and suitable fittings due to the flexible design of the overlapping layers, and the control of its stability and good behaviour [18].

Experimental Method

A nickel-alumina composite ($NiAl_2O_4$) was prepared by the chemical co-precipitation method with different weight ratios of the raw materials involved in the chemical reactions according to the formula $(NiO)_x(Al_2O_3)_{1-x}$, where x = 0, 0.125, 0.25, 0.375, and 0.5 g of the raw materials. The chemical materials that were used to synthesize the samples were Al $(NO_3)_3.9H_2O$ (Himedia, India, 95.0%), Ni $(NO_3)_2.6H_2O$ (AAG, Barcelona, 99.9%) and NH_4OH (Sigma Aldrich, Germany, 25%). A stoichiometric amount of the above weight ratios of both (Al $(NO_3)_3.9H_2O$) and ($Ni(NO_3)_2.6H_2O$) were dissolved in 100 ml. of distilled water. The solutions were mixed together in a beaker and slowly heated up to 60 ℃. A magnetic stirrer was used for 30 minutes to obtain homogeneity, and then a diluted solution of NH_4OH(10%) was added drop wise until the pH reached a value of 11-12.The obtained precipitate was separated, filtered, and washed with distilled water several times to remove the impurities and unreacted nitrates. It was then dried in an oven at 80 ℃ for 48 hours. The final precipitate powder was pre-calcined at 500 ℃ before being pressed into the form of pellets with a diameter of 12 mm using a pellet press (Specac, England) under a pressure of 3 ton/cm^2 for the A.C. measurements.

Finally, the powder was calcined in air at 1300 ℃ for 3 hours in a furnace (Carbolite, England). The furnace was then cooled slowly to room temperature at a rate of 10 ^{0}C /min. The structural characteristics of the prepared samples were determined by Fourier-transform infrared spectroscopy (FT-IR, model IR-Affinity, Shimadzu Corporation) in order to study the information concerning the different stretching and bending bonds of the nickel-alumina composite powder prepared by the chemical co-precipitation method.

The final product of the powder was analysed by means of the X-ray diffraction patterns obtained in the 2θ range of 20° to 60° using a Philips XRD-6000-Shimadzu diffractometer with Cu K*a* radiation (λ =1.5406 Å) operating at 40 kV and 30mA to identify the current phases. The dielectric properties as a function of the frequency in the range of 50 Hz–1MHz were investigated using an LCR-meter (LCR-8105G, Gwinstek, Thailand) to manufacture a laboratory-designed cell at room temperature. The dielectric constant (ε′) was calculated based on the following relationship [19]:

$$\varepsilon' = \frac{Cd}{\varepsilon_0 A} \quad (1)$$

Where, C is the capacitance, d is the thickness of the disc ε_0 is the permittivity of the free space, and A is the cross-sectional area of the disc.

The dielectric loss (ε″) was calculated according to the relationship [19]:

$$\varepsilon'' = \frac{1}{2\pi \cdot 1000 \cdot \varepsilon_0}\sigma \quad (2)$$

Where σ is the A.C. conductivity.

The dielectric loss tangent (tanδ) was calculated using the relationship:

$$\tan\delta = \frac{\varepsilon''}{\varepsilon'} \qquad (3)$$

Results and Discussion

Structural Properties

X-Ray Diffraction Spectroscopy

The XRD pattern for the α-Al_2O_3 powder, which had been prepared and calcined at 1300 ℃, was found to be that of pure α-Al_2O_3, which corresponded to the ICDD Standard Card No.00-010-0173, as shown in sample A, where the peak sites were identified accordingly, as shown in Fig. (1A). However, it was observed from the XRD pattern for sample N1 that there were two phases, corresponding to α-Al_2O_3 and $NiAl_2O_4$ through the angle of 19.1˚ belonging to the (111) plane, which referred to the phase formation of $NiAl_2O_4$, while the angle of 25.6˚ corresponded to the α-Al_2O_3 phase that had been formed, where the peaks sites corresponded with the two ICDD Card Nos.0-01-0-0 339 and 00-010-0173.

The results of the XRD pattern for the sample N1 which was being investigated showed the formation of an impurity phase of the powder due to the appearance of a peak at 25.6˚ which did not belong to the required powder but was the result of weak crystallization in the powder. This result corresponded with those reported by Hussein et al. [14] and Taylor et al., thereby indicating the formation of an impurity phase of Al_2O_3-$NiAl_2O_4$ [15]. The formation of an impurity phase in the powder occurred as a result of weak crystallization in the powder, which corresponded with the results obtained by Zangouei and others [16], as shown in Figure (1, N1).

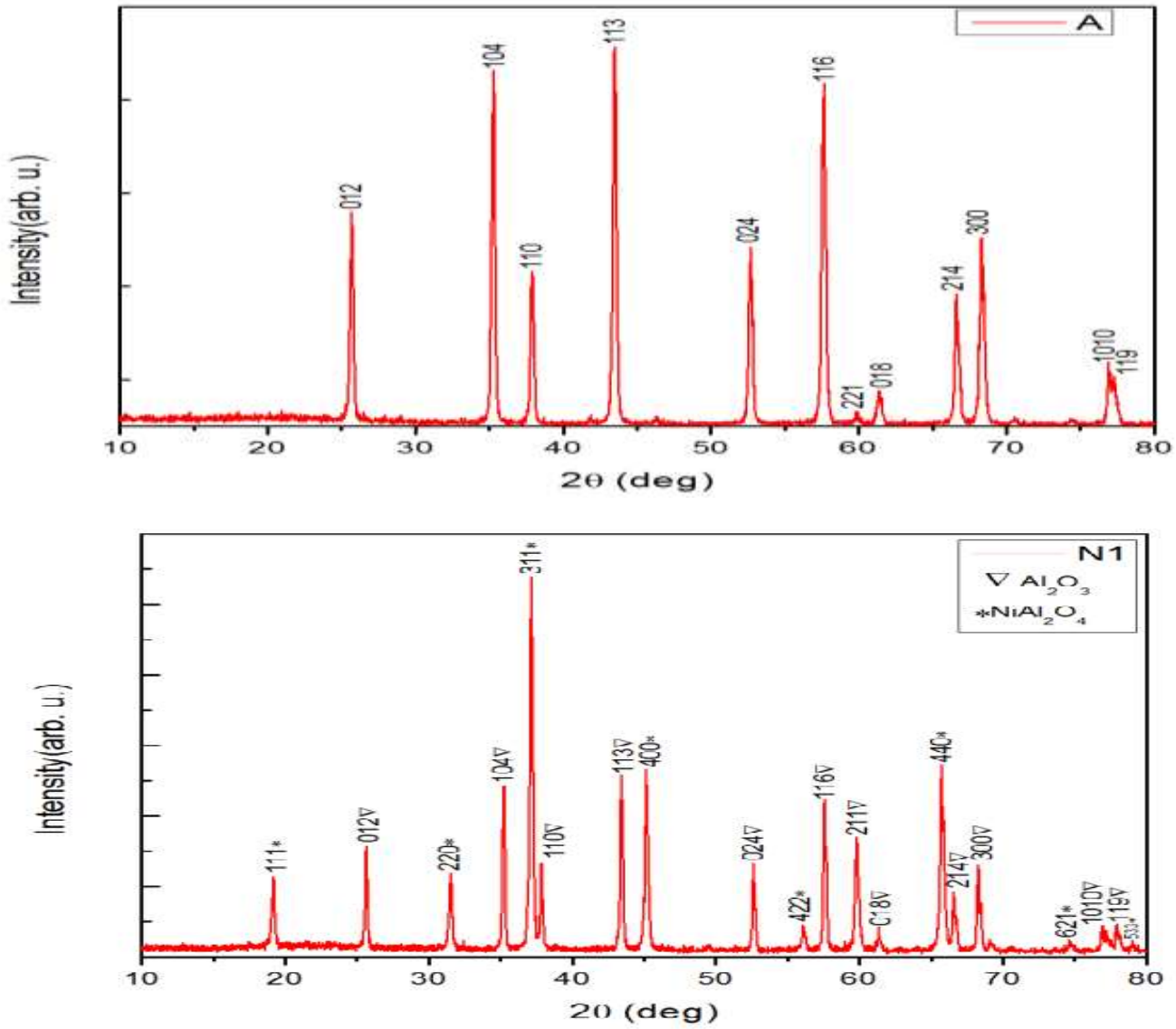

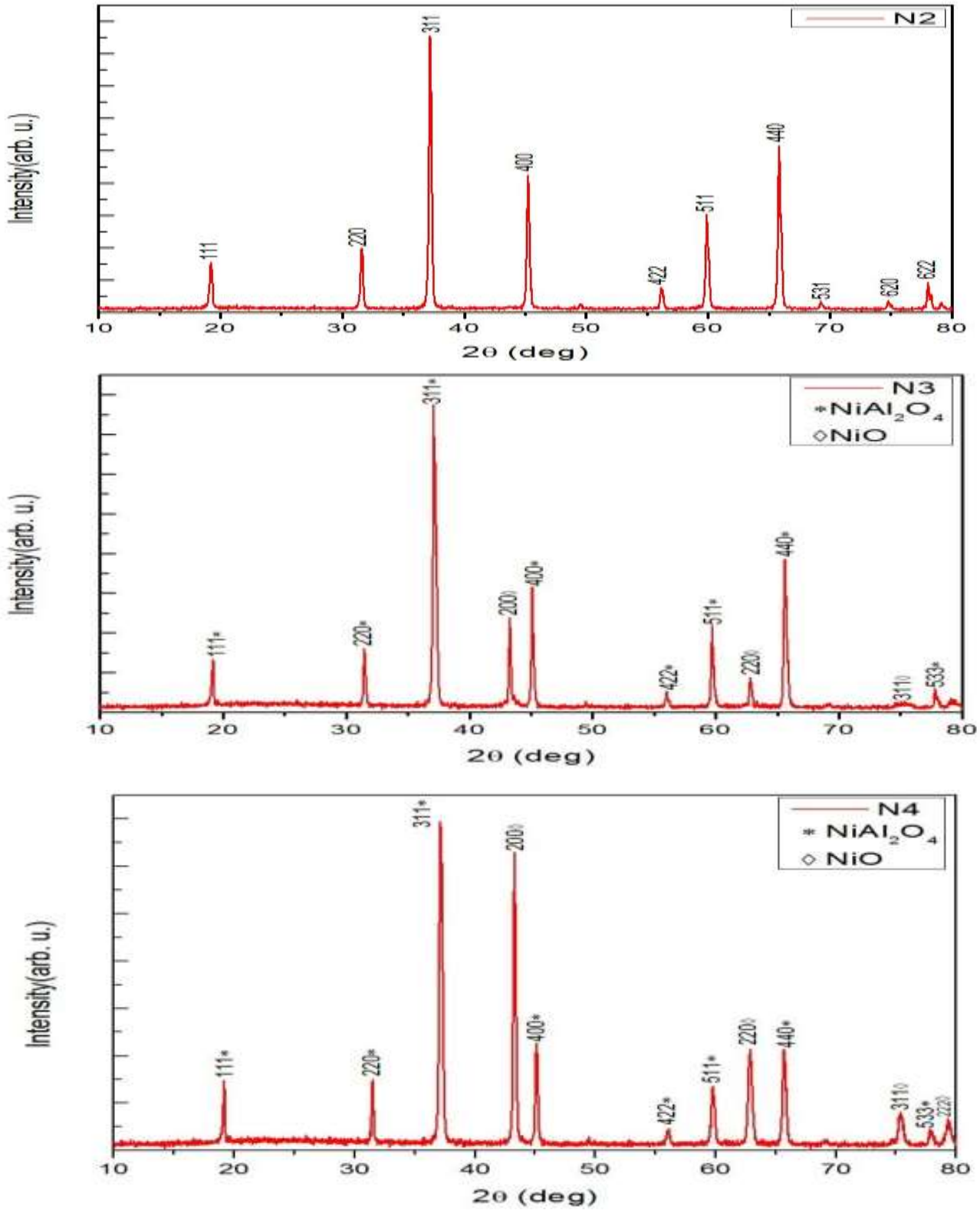

Figure 1: XRD Samples (A) Pure (α-Al_2O_3), N1 (Al_2O_3 / $NiAl_2O_4$), N2 ($NiAl_2O_4$), N3 (NiO / $NiAl_2O_4$)

The XRD pattern for the investigated sample, N2, showed the formation of only one phase in the prepared $NiAl_2O_4$powder, with no impurity phase of α-Al_2O_3being observed in the prepared powder. This corresponded entirely with the ICDD Standard Card No.00-010-0339.The above results can be interpreted in terms of the reaction mechanism that occurs when metal nitrates are decomposed by heat, where a lot of gases such as NO and NO_2 are emitted and may cause deformation of the attachments between the elementary particles involved in the chemical reaction. This, in turn, will prevent interactions. Therefore, the presence of NiO molecules, which had decomposed from the nickel nitrate, could have spread through the molecules of the alumina particles and their surface, thus resulting in the non-detection of the alumina particles during the XRD spectroscopy measurements as they had been transformed into the pure phase of the nickel alumina composite, as shown in the Figure (1,N2).This

corresponded with the results reported by Hussein et al., who investigated the effect of nitrogen oxide in the reaction to obtain the pure phase of the composite [14]. The XRD results for the other samples, namely N3 and N4, showed that the two phases of the prepared powders that were observed were those of $NiAl_2O_4$ and NiO, which corresponded with the ICDD Card Nos.00-010-0339 and 00-047-1049, where the presence of the impurity phase (NiO) corresponded with the results reported by Hi-bo et al., who explained that there are multiple phases involved in the formation of the same composite [17]. The crystallite sizes of the investigated samples were calculated through the use of the Scherer equation [20]:

$$D = \frac{k\lambda}{cos\theta\beta_{hkl}} \text{---------- (4)}$$

Where D is the average crystallite size of the phase, β is the Scherer constant for the full with half maximum (FWHM), λ (0.89) is the wave length of the X-ray beam used, and θ is the Bragg angle of diffraction. The calculation of the crystallite size of the prepared samples showed that the crystallite size of the $NiAl_2O_4$composite increased with an increase in the NiO ratio, where increasing the Al_2O_3 ratio caused an increase in the crystallite size, whereas the difference in the ionic radius between Al^{+3} (ion radius = 53 ºA) and Ni^{+2} (ion radius = 74 ºA) caused the crystallite size to increase [18]. However, the substitution sites between the Al^{+3} cations and Ni^{+2} cations in the crystalline lattice caused a crystalline defect, which may have been repeated to produce a lattice phase of the current $NiAl_2O_4$ composite or may be destructive to crystalline formation if the substitution ratio was large [21]. The following table shows the structural parameters of the α-Al_2O_3 and $NiAl_2O_4$ powders prepared by the chemical co-precipitation method.

Table 1: XRD spectroscopy parameters of (α-Al_2O_3) and ($NiAl_2O_4$)

sample	Code	hkl	2θ(deg)	FWHM(deg)	$d_{hkl}(^\circ A)$	Lattice constant $(a_\circ)\ ^\circ A$	D (nm)	Cell volume V_{cell} $(^\circ A^3)$
Al_2O_3	A	116	57.61	0.2596	1.59868	a=4.758, c=5.128	36.55	
$Al_2O_3/NiAl_2O_4$	N1	440	65.73	0.2196	1.41945	8.0297	44.99	518
$NiAl_2O_4$	N2	440	65.83	0.2083	1.41757	8.0184	47.46	515
$NiO/NiAl_2O_4$	N3	440	65.62	0.1994	1.42145	8.0411	49.5	520
$NiO/NiAl_2O_4$	N4	440	65.67	0.2811	1.42056	8.0362	35.13	519

FT-IR Spectroscopy

The FT-IR spectrum of the α-Al_2O_3 and $NiAl_2O_4$ composite powders, which were prepared with different ratios of the raw effective material and calcined at a temperature of 500ºC, explained that the extension vibrations of the free carboxyl group (C-O) bands were observed in the range of 1400 -1760 cm^{-1}.Thesecould be divided into two bands that appeared in the middle and at the terminals of the free carboxyl transmittance bands.

The first absorption band observed was close to the absorption bands at 1700cm^{-1}, which referred to the free carboxylic groups resulting from the acetone residues that were used for washing the samples before drying. Cracks were observed at the absorption bands of 1396.9cm^{-1} and 1644.52cm^{-1}, respectively, corresponding with the results reported by Geng et al. [22].

The absorption bands observed in the range of 700cm^{-1} to 900cm^{-1}were the result of the coordination between the Al^{+3} and Ni^{+2} cations, where the appearance of metal cations was due to an increase in the calcination temperature, which caused the transformation of the metal cations into oxides. The bands in the range of 590cm^{-1}were due to the metal-oxide vibrations of the spinal structure of the $NiAl_2O_4$ composite for all the samples, except for the formation of the aluminium oxide (Al-O) sample, as shown in Figure 3. At the final calcination temperature of 1300 °C, the appearance of absorbent bands was observed at 1000 cm^{-1}, which indicated the formation of the M-O spinal phase.

The absence of the absorption bands of the free carboxyl group (C-O) for all the samples meant that the impurities had been removed after the high-heat calcination, and the weak absorbance bands that appeared in the range of 2354cm^{-1}-2365cm^{-1}were due to the IR bands of the air between the source and the target. This was consistent with the findings of Nassar et al., Dash et al., Li et al. and Tripathy et al., which explained the reasons for the appearance of this band [23-26].

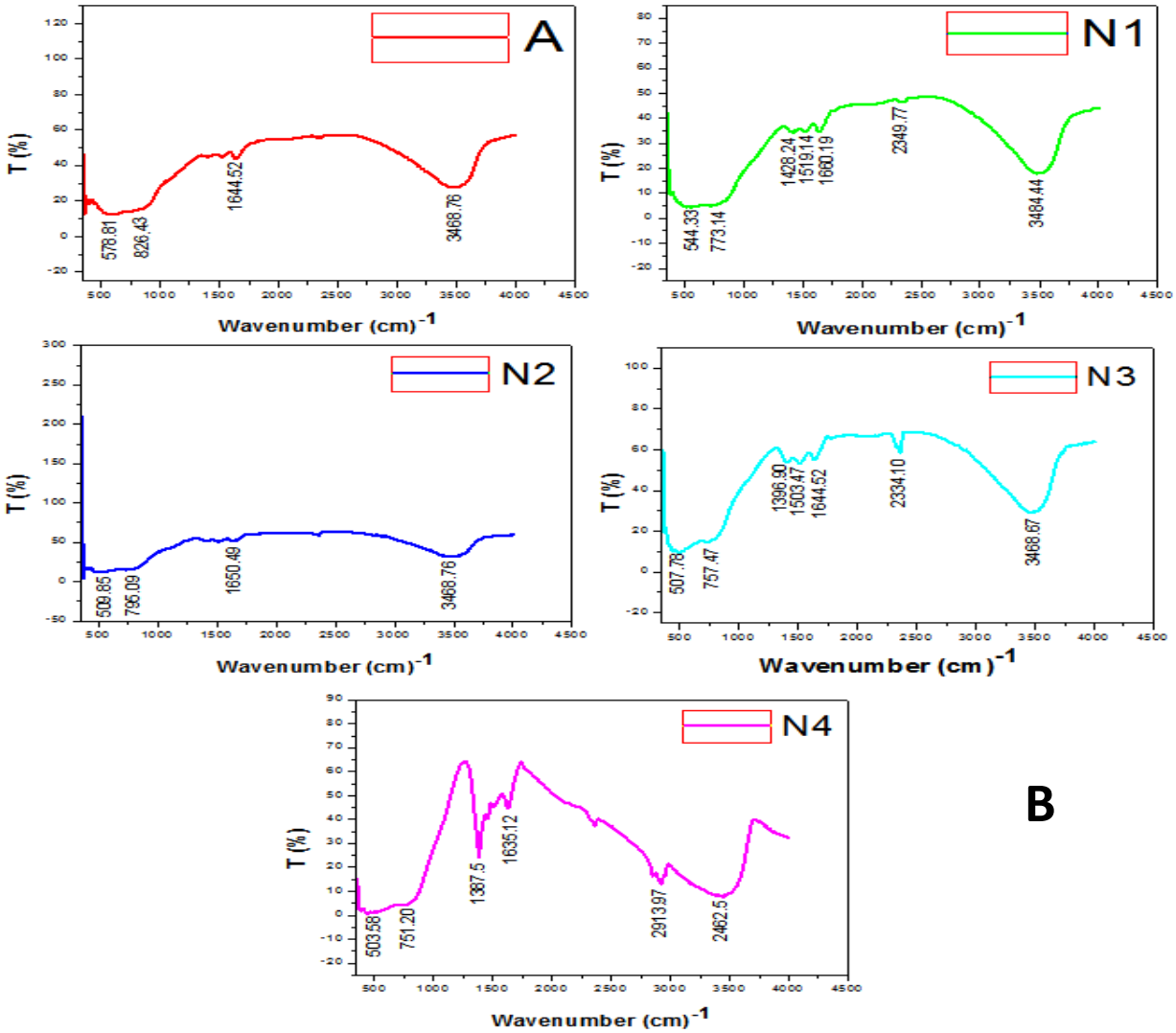

Figure 3: (FTIR) Spectrum A: at (500°C), B: at (1300 °C).

(A.C) Conductivity

The interaction of the external electric field with the dipoles of the dielectric materials in the A.C. conductivity measurements can be explained from the movement of the charge carriers through the dielectric materials, whereby the dielectric properties were studied as a function of the frequency, which had a strong relationship with the structure of the molecules. However, a change in the dielectric constant (ε') as a function of the frequency of the prepared samples of the $((NiO)_x (Al_2O_3)_{1-x})$ composite, as demonstrated in Figure (4A), showed thatε'decreased with an increase in the frequency, and it was independent of the

frequency at higher frequencies, where the dipole moments followed the external electric field at the low frequencies that arose from the different types of polarizations. However, at higher frequencies, the electric field did not change the direction of the ions due to the electronic exchange interaction in the ions. Kurien et al. observed a similar behaviour in the $NiAl_2O_4$ composite and suggested that the main reason for the higher dielectric constant at a low frequency was the ionic and space charge polarizations [28].From Figure (4B), the $\sigma_{a.c.}$vs (ω) plot showed two regions of conductivity or the measured frequency range. It was clear from Figure (4B) that there was an increase in the A.C. conductivity at a high frequency in the $NiAl_2O_4$ sample. The A.C. conductivity at a high frequency in the $NiAl_2O_4$sample was due to the hopping mechanism of the bound charges, whereby the free charges hopped back and forth between the well-defined bound states and hence, the A.C. conductivity increased at higher frequencies. In the spinal structure of the nanocrystalline $NiAl_2O_4$ sample, the presence of Al^{+3} ions in the octahedral sites and of Ni^{+2} ions in the tetrahedral sites was responsible for the electrical conductivity due to the transfer of electrons between the Al^{+3} and Ni^{+3} ions through the hopping conduction mechanism [29].

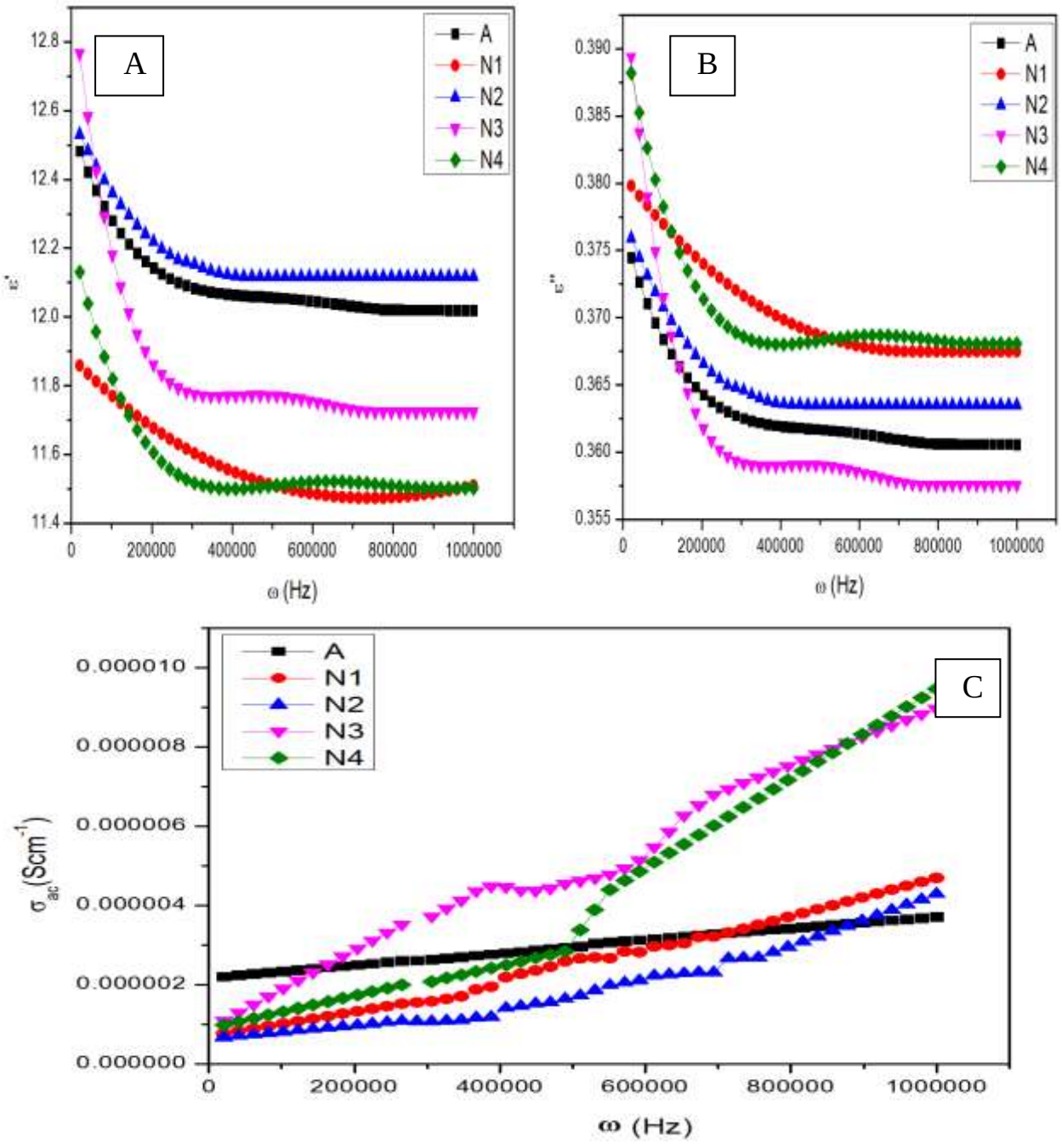

Figure 4: A, B: Real and imaginary dielectric constant; C: Electrical conductivity

Conclusion

The powders prepared by the chemical co-precipitation method with different weight ratios at a calcinations temperature of 1300 ℃ had multiple phases like NiO / $NiAl_2O_4$, $NiAl_2O_4$, α-Al_2O_3 / $NiAl_2O_4$. Thus, the best result of the $NiAl_2O_4$ composite was a major pure spinal phase formed at the ratio of x=0.25 at the high calcined temperature interaction between NiO and α-Al_2O_3. The α-Al_2O_3 had acrystallite size of 33nm, while the crystallite sizes of the Ni-substituted alumina composites were between 35 – 50nm, which increased with an increase in thenickel oxide content. The NiO and α-Al_2O_3 particles in the composite exhibited cubic and rhombohedral structures, respectively. In the composite, the lattice parameters were 4.15 Å for NiO while a = b = 4.75 Å, and c = 12.85 Å for α-Al_2O_3. The FT-IR investigations showed that the $NiAl_2O_4$ composite was formed in the spinal phase and inverse spinal phase through the formation of the NiO_4group in the tetrahedral sites and the AlO_6 group in the octahedral sites. The A.C. conductivity showed that the presence of the Al^{+3} ions in the octahedral sites and the Ni^{+2} ions in the tetrahedral sites was responsible for the electrical conductivity due to the transfer of electrons between the Al^{+3} and Ni^{+3} ions through the hopping conduction mechanism.

References

1. WD Kingery, HK Bowen, DR Uhlmann (1975) J, Wiley and Sons, Introduction to Ceramics, New York.
2. TA Ring (1996) Fundamentals of Ceramic Powder Processing and Synthesis, Academic Press 1st edition, Inc. San Diego.
3. K Niihara, T Hirai (1986) Ceramics, 26: 598.
4. M Sternitzke (1997) J. Eur. Ceram. Soc. 17: 1061.
5. Yuilun WU (2013) "Deposition of aluminum oxide by evaporative coating at atmospheric pressure {ECAP}", Master thesis of Science, Graduate College-University of Illinois at Urbana-Champaign, (1-8).
6. E Behravesh, L Hupa, T Salmi DY Murzin (2016) "Alumina ceramic foams as catalyst supports", Catalysis, (28-50).
7. Y Kathiraser, W Thitsartarn, K Sutthiumporn, S Kawi (2013) "Inverse $NiAl_2O_4$ on $LaAlO_3$-Al_2O_3: unique catalytic structure for stable CO2 reforming of methane", J. Phys. Chem, (8120-8130).
8. C Sprung, B Arstad, U Olsbye (2014) "Methane steam reforming over a Ni/$NiAl_2O_4$ model Catalyst – kinetics", Chem Cat Chem, 6:1969-1982.
9. K Babilius, A Babilius, L Jurgutis (2014) "Research of Ni-Al-O system catalytic coatings developed for gasification and steam reforming processes", Mechanics, 20.
10. IE Achouri, N Abatzoglou, C Fauteux-Lefebvre, N Braidy (2013) "Diesel steam reforming: comparison of two nickel aluminate catalysts prepared by wet-impregnation and co-precipitation", Catal. Today, 207 :(13-20).
11. IS Ahmed, HA Dessouki, AA Ali (2011) "Synthesis and characterization of $Ni_xMg_{1-x}Al_2O_4$ nano ceramic pigments via a combustion route", Polyhedron, 30 :(584-591).
12. C Jiménez-González, Z Boukha, B De Rivas, JJ Delgado, MÁ Cauqui, JR González-Velasco et al (2013) "Structural characterization of Ni/alumina reforming catalysts activated at high temperatures", Appl. Catal. Gen, 644: (9-20).
13. NM Ferreira, MC Ferro, SM Mikhalev, FM Costa, JR Frade, AV Kovalevsky et al (2016) "Guidelines to design multi component ferrospinels for high-temperature applications", Adv, 6:(32540-32548).
14. MM Hussein, IA Disher, SJ Idress (2017) "Synthesis of Stoichiometric phase pure $NiAl_2O_4$ using Molten Salt Method", International Journal of Applied Engineering Research, 12: 24 :(14818-14827).
15. N J Taylor, AJ Pottebaum, V UZ, RM laine (2014) "The bottom up approach is not always the best processing method: Dense α-Al_2O_3/$NiAl_2O_4$ Composites", Advanced Functional Material, (1-7).
16. M Zangouei, AZ Moghaddam, M Arasteh (2010) "The influence of Nickel loading on reducibility of NiO/Al_2O_3 catalysts synthesized by Sol-Gel method", 14 :(97-102).

17. Z Hai-bo, L Li-ming, X Di, Z Chu-guang, L Guo-jun, J Lin-lin (2008) "NiO/$NiAl_2O_4$ oxygen carriers prepared by sol-gel for chemical-looping combustion fueled by gas", journal of fuel chemistry and technology, 36:(261-267) .
18. Jan Harloff (1995) "In-situ quantitative measurement of electric fields in zinc oxide thin films using electrostatic force microscopy", A Master theses of Science, University of Pennsylvania, (14-18).
19. MH Diwan, NA Bakr , F Jamali-Sheini (2014) structural and dielectric Studies of cobalt ferrite nanopowder prepared by ceramic method; International Journal of Current Research, 6(01):4562-4566.
20. BD Cullity (1976) Elements of X-ray Diffraction, Addison-Wesly Publishing Co. Inc. (Chapter 14).
21. Muayad J (1987) Yusif, "Solid state physics – part 1", 2nd Edition, (138).
22. Q Geng, X Zhao, X Gao, S Yang, G Liu (2012)"Low-temperature combustion synthesis of $CuCr_2O_4$ spinel powder for spectrally selective paints", J. Sol-Gel Sci. Technol, 61:(281-288).
23. MY Nassar, IS Ahmed, I Samir (2014)" A novel synthetic route for magnesium aluminate ($MgAl_2O_4$) nanoparticles using sol-gel auto combustion method and their photocatalyticproperties, Spectrochim", Acta, 131 :(329-334).
24. S Dash, RK Sahoo, A Das, S Bajpai, D Debasish, SK Singh (2017) "Synthesis of $MgAl_2O_4$ spinel by thermal plasma and its synergetic structural study", J. Alloy. Compd, 726 :(1186-1194).
25. H Li, H-Y Wei, Y Cui, R-L Sang, J-L Bu, Y-N Wei, J Lin, J-H Zhao (2017) "Synthesis and characterisation of $MgAl_2O_4$ spinel nanopowders via nonhydrolytic sol-gel route", J. Ceram. Soc. Jpn. 125 :(100-104).
26. S Tripathy, DS Saini, D Bhattacharya (2017) "Synthesis and Fabrication of $MgAl_2O_4$ ceramic foam via a simple, low-cost and eco-friendly method", J. Asian Ceram, 4 :(149-154).
27. J Ahmed, SH Bukhari, MQ Awan, ME Mazhar, AR Makhdoom (2018) "Dielectric and impedance spectroscopy of K^+- doped $MgAl_2O_4$ nanoparticles", International Journal of Modern Physics B, 32:(1-13).
28. S Kurien, S Sebastian, J Mathew, KC George (2004) "Structural and Electrical properties of nano-size magnesium aluminate", Indian Journal of Pure & Applied Physics, 42 :(926-936).
29. SS Atta-Allah, MK Fayek (2000)"Effect of Cu substitution on Conductivity of Ni–Al ferrite", J. Phys. Chem. Solids, 61:1529-1534.

